

## Direct structural evidence of the change in N-III bonding in (GaIn)(NAs) before and after thermal annealing

K. Volz,<sup>a)</sup> T. Torunski, O. Rubel, and W. Stolz

*Materials Science Center, Central Technology Laboratory, Philipps University Marburg, Marburg 35032, Germany*

(Received 5 February 2008; accepted 23 June 2008; published online 4 September 2008)

The blueshift of the fundamental energy gap of (GaIn)(NAs) upon thermal treatment is well established. However, the physical reason is still controversially discussed in literature. In the present paper we give direct structural evidence using transmission electron microscopy in combination with structure factor calculation that this blueshift—for the metal organic vapor phase epitaxy grown samples investigated here—results solely from a change in the local environment of nitrogen. N is bound to Ga upon growth and moves into an In-rich environment upon annealing to minimize the strain energy of the crystal. The technique presented here can be used to unambiguously determine the reason for the blueshift of differently grown and annealed dilute nitride materials. © 2008 American Institute of Physics. [DOI: [10.1063/1.2970162](https://doi.org/10.1063/1.2970162)]

### I. INTRODUCTION

The dilute N containing quaternary alloy (GaIn)(NAs) is of considerable technological interest as the N induces a theoretically predicted<sup>1,2</sup> and experimentally proven<sup>3–5</sup> strong bowing of the band gap in this material system and hence allows for emission wavelengths in the range of 1.3–1.55  $\mu\text{m}$  on GaAs substrates. (GaIn)(NAs) grown lattice matched to GaAs or Ga with a 1 eV band gap is also a candidate for one of the junctions in III/V multijunction solar cells.<sup>6</sup>

The metastable (GaIn)(NAs) material system is characterized by several unique effects observed as a consequence of postgrowth thermal treatment. Annealing in this material system results—from the optoelectronic point of view—on one hand in a dramatic increase in luminescence intensity. The reason for that is not completely understood yet.<sup>7–16</sup> On the other hand, one observes a blueshift of the fundamental energy gap after annealing, which is controversially discussed in literature. The magnitude of the blueshift depends on In and N contents in the samples, but is commonly highest for high In and N contents and can be as large as 100 meV. The blueshift of the fundamental energy gap is observed irrespective of the growth technique used. However, there might be several mechanisms contributing to an increase in the band gap of the material. Some of those are growth technique and annealing related, e.g., element diffusion on both group-III and group-V sublattices, altering the composition of the structures. Some of the mechanisms are intrinsic for the material systems under investigation, e.g., local atomic ordering. The magnitude of the various contributions strongly depends on the growth conditions [e.g., molecular beam epitaxy (MBE) or metal organic vapor phase epitaxy (MOVPE), choice of precursors and N and In concentrations] as well as the annealing conditions (annealing time, ambient, annealing temperature, etc.).

There are several reports in the literature dealing with

the compositions of the quaternary material before and after annealing. Various papers report that the composition of the alloy does not change upon annealing. This is mainly seen by high-resolution x-ray diffraction (HRXRD) analysis.<sup>17,18</sup> After different growth and annealing procedures, however, atom diffusion on the group-III and group-V sublattices can also take place. It was demonstrated in Ref. 15 that inhomogeneities in the In composition throughout the quantum wells (QWs), which were present after MBE growth, can be dissolved upon annealing, resulting in a reduction of the maximum In concentration after annealing. It is shown that the blueshift and the reduction in photoluminescence (PL) linewidth and in Stokes shift are related to the In distribution homogenization. Rapid thermal annealing (RTA) is also shown to result in N diffusion out of the QW.<sup>19</sup> The blueshift of the PL in these samples is due to a reduced N concentration in the QWs upon annealing. Similar element redistribution effects upon annealing were also observed by other groups.<sup>17,20</sup>

Strong QW/barrier intermixing (which was mainly observed for MBE-grown samples<sup>7,9,12</sup>) can be caused by the enhanced presence of point defects (which originate from the rf nitrogen plasma source used for incorporating N in MBE). Sun *et al.*<sup>21</sup> showed the secondary ion mass spectrometry of MBE samples that intentionally introducing point defects in the material results in the interdiffusion of group-III atoms between the QWs and barriers, and hence in a blueshift of the PL signal. It is also possible that point defects promote—in addition to interdiffusion—in-plane compositional diffusion.

Several authors even reported on a redshift of the PL emission upon RTA of MBE-grown samples.<sup>22</sup> The activation of N from interstitial to substitutional sites may be responsible for this redshift. It was shown by a combination of nuclear-resonance analysis and ion-beam channeling that a significant amount of N is incorporated on interstitial lattice sites during MBE growth.<sup>23</sup> This interstitial N is removed upon annealing. It can be either activated to lattice sites or

<sup>a)</sup>Electronic mail: kerstin.volz@physik.uni-marburg.de.

diffused out of the sample completely. The authors also observe an outdiffusion of substitutional nitrogen upon RTA that could also explain some of the blueshift of RTA annealed MBE-grown samples. Those studies show that—depending on growth and annealing conditions used—it is possible to keep the QW composition unchanged or alter it after annealing for both growth and annealing techniques used, the latter of which already can introduce a significant blueshift to the PL signal.

An intrinsic contribution to the blueshift, however, is the rearrangement of the local N environment as it does not alter the macroscopic composition of the crystal. A single (GaIn)(NAs) crystal with a fixed composition was shown to possess five different band gaps caused by five different nearest-neighbor (NN) environments of N.<sup>14</sup> The NN environment of N and the band gap of the material can be tuned by changing the annealing conditions.

The direct structural proof of the N environment in mixed crystals containing only dilute amounts of N is difficult to bring forward. There are reports in literature on the local mode spectroscopy of as-grown and annealed MOVPE-grown (GaIn)(NAs) solar cell and laser material,<sup>16,17,24–26</sup> which show the increase in an In–N mode after annealing, whereas upon growth Ga–N modes are mainly detectable. Very convincing evidence for such changes is obtained by Raman spectroscopy close to the  $E+$  resonance with excitation energies of 2.18 eV (Ref. 16) and 1.92 eV.<sup>25</sup> Other proof includes extended x-ray absorption fine structure (EXAFS) measurements in combination with *ab initio* simulations on MBE-grown (GaIn)(NAs) laser material.<sup>27,28</sup> These EXAFS data and the theoretical calculations are still discussed controversially in the literature,<sup>29</sup> where only one order of magnitude weaker ordering than predicted in Ref. 30 is anticipated. It is worth mentioning that under certain growth and annealing conditions there seems to be no significant changes in the NN environment of N in (GaIn)(NAs); i.e., the 4Ga environment dominates even after annealing.<sup>31</sup>

In the following, a different and direct way of proving the change in N environment or any element redistribution upon annealing is presented and discussed. Composition-sensitive transmission electron microscopy (TEM) dark field micrographs in combination with refined structure factor calculation, together with strain-state analysis of as-grown and annealed (GaIn)(NAs), will be presented. As these investigations were performed on laser material with an In content of 30% and a N content of 1.5% (lattice mismatch to GaAs, 3.6%), as well as on solar cell material (lattice matched to GaAs) with In content of 8% and N content of 3%, they confirm that the structural changes in NN scale happen in the structures under investigation here. Moreover, the novel technique presented here can be used to unambiguously determine all the reasons for the PL shift in any (GaIn)(NAs) samples upon annealing.

## II. EXPERIMENTAL

(GaIn)(NAs)/GaAs multiquantum well (MQW) structures have been grown on (001) GaAs substrates by MOVPE in a commercial reactor system (AIX200-GFR) under  $H_2$

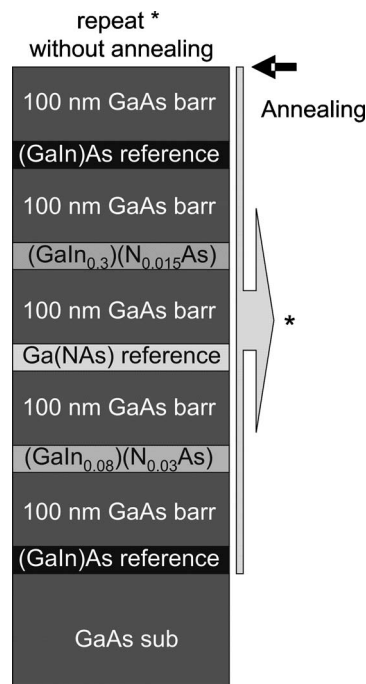


FIG. 1. Schematic cross section of the TEM sample structure.

carrier gas at a reduced pressure of 50 hPa. As one deals with a metastable material system, nonequilibrium growth conditions, i.e., low substrate temperatures, have to be employed and more efficient decomposing group V precursors [tertiary butyl arsine (TBA) and 1,1-dimethylhydrazine] have been used. (GaIn)(NAs) laser material, which would emit at the 1.3  $\mu\text{m}$  range, has a composition of about 30% In and 1.5% N. (GaIn)(NAs) solar cell material, which is lattice matched to GaAs and has a 1 eV band gap, has an In content of 8% and a N content of 3%. Annealing of the structures took place in the MOVPE reactor using a procedure that was optimized for maximum PL efficiency gain of laser structures (700 °C for 5 min under TBA stabilization and 25 min at +625 °C unstabilized in  $H_2$  ambient).

Structures for TEM were MQWs with 100 nm wide GaAs barriers in order to ensure that any strain contrast caused by the deformation of the thin TEM sample and even visible in  $g=(002)$  dark field images<sup>32,33</sup> does not influence the subsequent QW intensity. QW thicknesses were in the range of 10–20 nm, depending on the strain with respect to the substrate. The TEM samples consist of QWs with different compositions in one single sample to ensure identical sample preparation conditions and imaging conditions for all the layers under investigation. As the (002) dark field intensity for several quaternary compositions does not show the zero-intensity transition at the interfaces of the QWs, special  $(Ga_{0.7}In_{0.3})As$  QWs with a composition gradient at both interfaces were grown into the sample to have the intensity zero of the charge coupled device (CCD) camera, which needs to be subtracted from the dark field intensity before further processing. This design was chosen to definitely include the zero-intensity value, which is around 20% In. A schematic cross section of the used sample structure is shown in Fig. 1. For reference purposes (PL and XRD measurements), five time QW structures of the different materials

were also deposited and in part annealed under identical conditions as the TEM sample. The [010] TEM cross sections were prepared by mechanical polishing followed by 3 and 1 kV Ar ion milling, as well as by cleavage techniques. The  $g=(002)$  dark field images were obtained in a JEOL JEM3010 at an acceleration voltage of 300 kV, tilting the samples around the growth direction away from the [010] pole so that only the transmitted and the (002) beams were excited strongly. In the geometry used, the center of Laue circle was corresponding to (20, 0, 1) to (20, 0, 1.5) for the (002) reflection, resulting in low influence of small thickness fluctuations of the samples on the observed image intensity. To get a measure for the error bar of these measurements, several ( $>10$ ) measurements were undertaken at different sample positions, i.e., different sample thicknesses. From the values derived, an error bar was calculated. For strain-state analysis from high-resolution images, the samples were tilted to the same direction and the direct (000) beam was allowed to interfere with the diffracted (002) beam to obtain a stripe image. From the distance of the stripes one can derive the tetragonal distortion of the QWs if—in case of strained films—the results are compared to finite element simulation of the strain state of the thin TEM sample. For HRXRD a five crystal diffractometer was used and  $\omega-2\theta$  scans were recorded around the (004) reflection of the substrate. The PL of the reference samples was measured at room temperature, using a 514 nm cw Ar ion laser for excitation. The emission of the samples was dispersed in a 1 m grating monochromator (THR 1000 from Jobin-Yvon) for evaluation of the spectral characteristics.

### III. RESULTS AND DISCUSSION

We will show first that annealing our MOVPE-grown (GaIn)(NAs) results in the well-known changes in the optical characteristics as the blueshift of the band gap. The structure factor calculations, which base the TEM dark field analysis, will be described in the following, and we will show that annealing did not change the macroscopic strain state for all (GaIn)(NAs) alloys under investigation here. Measuring the intensity across dark field transmission electron micrographs and comparing these results with structure factor calculations, we will provide a direct structural proof of the N site change upon annealing from a Ga-rich environment to an In-rich one.

#### A. PL characteristics

The blueshift of the band gap of (GaIn)(NAs) with different compositions is shown as a function of the In content in the material in Fig. 2. The blueshift increases with increasing In content in the layers. The theoretical values for the blueshift of N in different group-III environments derived from Ref. 14—under the assumption that the only reason for the blueshift of the band gap is the change in the NN environment of the N—are indicated as dashed lines in this figure. The values of N with one (blueshift of 20 meV), two (blueshift of 40 meV), or three (blueshift of 60 meV) In NNs after annealing are given for a N content of 1.5%. The amount of blueshift increases with increasing In content (as

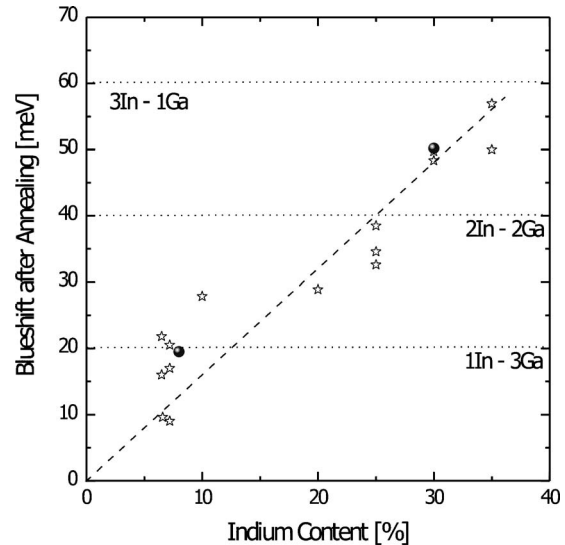


FIG. 2. Blueshift of (GaIn)(NAs) QW structures having different In contents as a function of the In content in the material.

well as with increasing N content) due to the increasing number of In-rich bonding sites available for a group-V atom from a statistical distribution of the In. The two samples analyzed in this study are  $(\text{Ga}_{0.92}\text{In}_{0.08})(\text{N}_{0.03}\text{As}_{0.97})$  solar cell material and  $(\text{Ga}_{0.7}\text{In}_{0.3})(\text{N}_{0.015}\text{As}_{0.985})$  laser material, which are shown in the figure as dots. Before annealing, both materials had N solely in Ga environment (N-4Ga). The solar cell material has after annealing the N on average in one In environment (blueshift of 19.9 meV: configuration N-1In3Ga), whereas the (GaIn)(NAs) laser sample has between two and three In NNs of the N (blueshift of 50 meV: configuration 50%N-2In2Ga+50%N-3In-Ga). These statistical values for the N-III bonding arrangement enter the later valence force field (VFF) calculations of the local lattice strain, which is needed for the structure factor calculations.

#### B. Structural characterization

##### 1. Structure factor calculation

Imaging crystals with zinc-blende symmetry using  $g=(002)$  in a TEM are characterized by chemical sensitivity of the dark field micrograph. The strong influence of the composition on the image intensity can be concluded when studying the structure factor. The square of the absolute value of the structure factor is proportional to the image intensity in kinematical approximation,

$$I(\mathbf{g}) \sim |F(\mathbf{g})|^2. \quad (1)$$

The value of the structure factor  $F$  for a particular reflection  $\mathbf{g}=(hkl)$  can be expressed in the form

$$F(\mathbf{g}) = N^{-1} \left\{ \sum_j f_j(\mathbf{g}) \exp[2\pi i \mathbf{g}(\mathbf{r}_j + \mathbf{u}_j)] \right\}, \quad (2)$$

where  $N$  is the number of unit cells over which we average the structure factor,  $f_j(\mathbf{g})$  is the kinematic electron scattering factor, and  $r_j$  is the average crystal sites of the atoms. In a virtual average crystal, group-V atoms occupy sites with coordinates  $r_V=(0,0,0)$ , whereas group-III atoms are located

TABLE I. Comparison of the calculated and experimentally determined image intensities of (GaIn)(NAs) laser and solar cell material, respectively. To obtain the theoretical image intensity ratios, it has been assumed that the nitrogen changes its environment from a Ga-rich one upon growth to an In-rich one upon annealing (ann). The values for the different NN environments of the N are indicated.

Material system	Theory					Experiment $I_{\text{ann}}/I_{\text{asgrown}}$
	N-4Ga0In	N-3Ga1In	$ F_{002} _{\text{ann}}^2/ F_{002} _{\text{as-grown}}^2$	N-2Ga2Ga	N-1Ga3Ga	
Solar cell $\text{Ga}_{0.92}\text{In}_{0.08}\text{N}_{0.03}\text{As}_{0.97}$	1	$1.16 \pm 0.02$	$1.19 \pm 0.02$	$1.19 \pm 0.02$	$1.19 \pm 0.02$	$1.17 \pm 0.05$
Laser $\text{Ga}_{0.7}\text{In}_{0.3}\text{N}_{0.015}\text{As}_{0.985}$	1	$0.88 \pm 0.02$	$0.83 \pm 0.02$	$0.83 \pm 0.02$	$0.83 \pm 0.02$	$0.85 \pm 0.05$

at  $r_{\text{III}}=(0.25,0.25,0.25)$ . As a consequence of the small atomic radius especially of nitrogen, the atoms might be displaced from their virtual average position  $r_j$  by a vector of static atomic displacement  $u_j$ . This is important to take into account as has already been demonstrated for Ga(NAs)/GaAs.<sup>33</sup> The kinematic electron scattering factors of individual atoms calculated by Doyle and Turner<sup>34</sup> were used in the following calculations. In order to compute the atomic displacement  $u_j$ , we employed the VFF supercell method described previously.<sup>35</sup> A supercell with size of  $40 \times 40 \times 40$  unit cells showing adequate convergence for the structure factor was used. First, the atomic species were placed at their “ideal” positions and  $r_j$  in the virtual crystal, taking into account the tetragonal distortion. Then the atomic coordinates were relaxed with respect to the total strain energy in accordance with Keating’s<sup>36</sup> VFF model. As one deals with a quaternary alloy, having a mixed group-V as well as group-III sublattice, the structure factor of the alloy will be different, whether one treats it to be GaN+InAs-like (“as grown”) or InN+GaAs-like (“annealed”). This difference arises mainly from the different bond lengths of InN versus GaN. Interaction parameters for GaAs, InAs, InN, and GaN used in the strain energy functional are listed in Ref. 37. During the relaxation procedure we applied additional constraints in order to keep the macroscopic strain of the supercell constant. The structure factors for the  $g=(002)$  vector were calculated for solar cell material (In=8%, N=3%) as well as laser material (In=30%, N=1.5%). A random indium distribution was assumed for both compositions and irrespective of the thermal treatment. The difference between the as-grown and annealed atomic arrangements is the distribution of the nitrogen atoms. In the case of the as-grown alloy, nitrogen atoms were distributed randomly among the group-V lattice sites, which have no indium in the first NN shell. The annealed alloys were generated by filling the nitrogen atoms in lattice sites with In in the first NN shell. The annealed alloys were simulated with different numbers of In atoms in the first NN shell of the N. The intensity of the quaternary alloy should be different when the nearest neighborhood arrangement of the nitrogen changes. The square of the absolute value of the structure factor, calculated for different N-III neighborhoods, was normalized to the square of the absolute value of the structure factor, assuming that N is exclusively bound to Ga. These numbers are given in Table I. The normalization took place in order to ensure comparability to the later experiments. It can be seen that the contrast of

solar cell material becomes brighter if the nitrogen place change happens, whereas the laser material becomes a darker contrast. The largest intensity change is already expected when the N changes its environment from 4Ga to 3Ga1In. Aside from this conclusion, the discrimination between different In-rich NN environments can only be done if the experimental error is very low.

## 2. Determination of lattice constant

These changes in image intensity and hence in structure factor can of course be only differentiated from an altered chemical composition if one proves that the composition before and after annealing stayed unchanged. This was performed in several ways, two of which will be elucidated in the following. To show that the quaternary composition did not alter upon annealing—under the conditions used here—the tetragonally distorted lattice constant of the QWs was measured from high-resolution TEM images before and after annealing. If one takes the thin foil relaxation into account when dealing with strained laser samples, this gives direct information whether the composition of the QW did alter. Relaxation of the thin TEM specimen does not need to be taken into account when dealing with lattice matched solar cell material. A comparison of the lattice constants in growth direction of a lattice matched (GaIn)(NAs) QW before and after annealing for 5 min at 700 °C under TBA stabilization and subsequently for 25 min at 625 °C without any stabilization is shown in Fig. 3(a). It can be seen that the lattice constant of the (GaIn)(NAs) is identical to the one of the GaAs, proving first that the lattice matching conditions, which were aimed for, are actually fulfilled. Furthermore, there is also no difference in strain state between the as-grown and annealed samples, proving that the chemical composition of the quaternary alloy did not alter upon annealing, neither did the interface structure of the QW with the GaAs barriers. It was also shown for laser material in the same way that the composition did not change upon annealing. In addition to this nanoscale analysis of strain, it was shown by HRXRD that the macroscopic strain state of the material did not change upon annealing.  $\omega$ -2 $\theta$  HRXRD scans around the (004) GaAs reflection of a  $(\text{Ga}_{0.7}\text{In}_{0.3})(\text{N}_{0.015}\text{As}_{0.985})$  MQW structure before and after annealing are shown in Fig. 3(b). The Pendellösung fringes are well established in both diffraction patterns and the superlattice reflections are at identical positions. This confirms that no QW-barrier intermixing

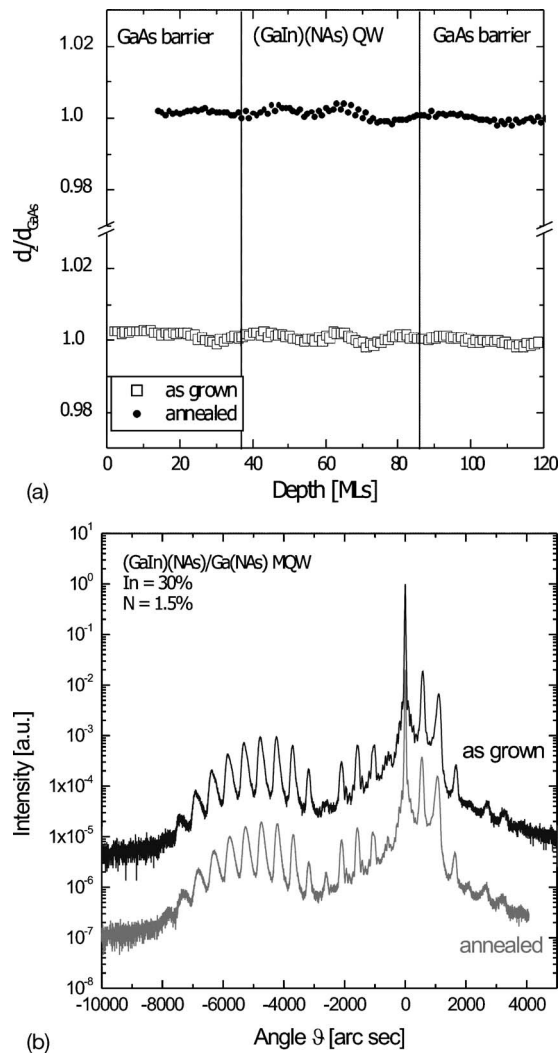


FIG. 3. (a) Strain-state analysis of a  $(\text{Ga}_{0.92}\text{In}_{0.08})(\text{N}_{0.03}\text{As}_{0.97})$  QW before (open symbols) and after annealing (filled symbols). (b) HRXRD  $\omega$ - $2\theta$  scans of a  $(\text{Ga}_{0.7}\text{In}_{0.3})(\text{N}_{0.015}\text{As}_{0.985})$  MQW structures before and after annealing.

took place and that the interfaces of both samples are equally sharp. As the position of the QW envelope also did not change upon annealing, one can further conclude that the average QW composition stayed unchanged upon the applied annealing.

### 3. Chemically sensitive TEM dark field

Bearing this study in mind, one can now investigate the chemically sensitive  $g=(002)$  dark field micrographs, which ought to give information on the local environment of the nitrogen as explained above. The  $(002)$  dark field micrographs of  $(\text{GaIn})(\text{NAs})$  laser, as well as solar cell material (a) before and (b) after annealing, are shown in Figs. 4 and 5. Line scans across the respective images are shown in (c). It can be seen that for the laser material the image intensity decreased upon annealing, whereas for solar cell material the image intensity increased upon annealing. To derive quantitative information from these intensity scans, the “zero value” for the CCD camera, which was obtained from the interfacial layers of the  $(\text{GaIn})\text{As}$  reference QWs, was subtracted from the respective image intensities. As the sample

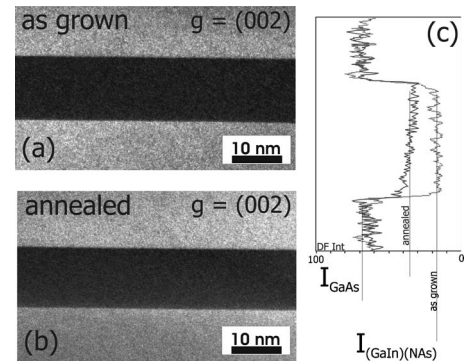


FIG. 4. Composition-sensitive  $(002)$  DFTEM images of a  $(\text{Ga}_{0.92}\text{In}_{0.08})(\text{N}_{0.03}\text{As}_{0.97})$  QW (a) before and (b) after annealing. The line scans across the images are depicted on the right hand side.

contains four  $(\text{GaIn})\text{As}$  reference QWs distributed over the complete region of interest, this procedure is more accurate than subtracting the zero intensity, which one would derive from the dark field (DF) intensity of the hole of the TEM specimen. To exclude the effects of sample thickness, these corrected intensities were afterwards divided by the intensity of  $\text{GaAs}$  neighboring regions. This results in zero-intensity-corrected and thickness-normalized  $(002)$  DF intensities for the  $(\text{GaIn})(\text{NAs})$  QWs, which can be further processed.

### 4. Comparison of experiment and theory

The experimentally determined intensity changes upon annealing are quantified in Table I and compared to the calculated intensities. The numbers given in Table I are the ratios of squared values of absolute numbers of structure factors for nitrogen configurations before and after annealing, together with the ratios of the respective dark field image intensities for both solar cell and laser material. There is an excellent agreement between the theoretical values assuming the NN change in nitrogen from a Ga-rich to an In-rich environment upon annealing and the experimental data. These results are a direct nanostructural proof that the N changes its environment from a Ga-rich one upon growth to an In-rich one after annealing. The driving force for this NN change is the reduction in strain energy of the crystal.<sup>37</sup>

### IV. SUMMARY

In summary, this study gives direct structural evidence that the supposed change in local environment of the N ac-

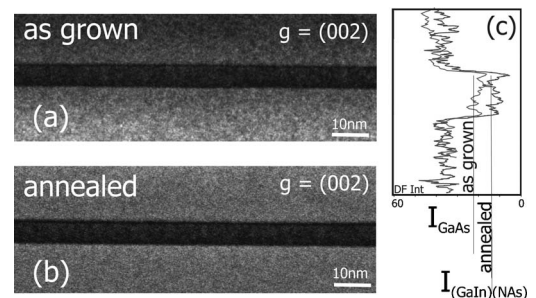


FIG. 5. Composition-sensitive  $(002)$  DFTEM images of a  $(\text{Ga}_{0.7}\text{In}_{0.3})(\text{N}_{0.015}\text{As}_{0.985})$  QW (a) before and (b) after annealing. The line scans across the images are depicted on the right hand side.

tually takes place driven by the strain energy of the crystal. The samples investigated here were grown by MOVPE and did not show a change in macroscopic strain state, interface configuration, and thickness of the QWs after annealing, indicating that the composition remained unchanged upon annealing. Using chemically sensitive dark field imaging in a TEM in combination with refined structure factor calculation, it can directly be shown that the N changes its site upon annealing from a Ga-rich one upon growth to In-rich environments. This can be detected by dark field TEM (DFTEM) as Ga-rich and In-rich environments of the N are characterized by different bond lengths, as also calculated by VFF methods. The bond lengths in the crystal enter the structure factor, the square of which is directly proportional to the DF intensity.

As the method presented here is not only sensitive to the local rearrangement in the N environment but also capable of detecting changes in (GaIn)(NAs) QW composition and strain state, it can be used for all (GaIn)(NAs) structures to unambiguously determine the reasons for the PL shift of the respective samples.

## ACKNOWLEDGMENTS

Financial support of the German Science Foundation in the framework of the topical research group "Metastable Compound Semiconductors and Heterostructures" is gratefully acknowledged.

- <sup>1</sup>S. H. Wei and A. Zunger, *Phys. Rev. Lett.* **76**, 664 (1996).
- <sup>2</sup>M. Kondow, T. Kitatani, S. Nakasuka, M. C. Larson, K. Nakahara, Y. Yazawa, M. Okai, and K. Uomi, *IEEE J. Quantum Electron.* **3**, 719 (1997).
- <sup>3</sup>L. Bellaiche, *Appl. Phys. Lett.* **75**, 2578 (1999).
- <sup>4</sup>F. Höhnsdorf, J. Koch, C. Agert, and W. Stolz, *J. Cryst. Growth* **195**, 391 (1998).
- <sup>5</sup>M. Weyers, M. Sato, and H. Ando, *Jpn. J. Appl. Phys., Part 2* **31**, L853 (1992).
- <sup>6</sup>S. R. Kurtz, D. Myers, and J. M. Olson, in Proceedings of the 26th IEEE Photovoltaic Specialists Conference (IEEE, New York, 1997), p. 875.
- <sup>7</sup>Z. Pan, L. H. Li, W. Zhang, Y. W. Lin, R. H. Wu, and W. Ge, *Appl. Phys. Lett.* **77**, 1280 (2000).
- <sup>8</sup>S. Francoeur, G. Sivaraman, Y. Qiu, S. Nikishin, and H. Temkin, *Appl. Phys. Lett.* **72**, 1857 (1998).
- <sup>9</sup>I. A. Buyanova, G. Pozina, P. N. Hai, N. Q. Thing, J. P. Bergman, W. M. Chen, H. P. Xin, and C. W. Tu, *Appl. Phys. Lett.* **77**, 2325 (2000).
- <sup>10</sup>T. Kitatani, K. Nakahara, M. Kondow, K. Uomi, and T. Tanaka, *J. Cryst. Growth* **209**, 345 (2000).
- <sup>11</sup>P. Gilet, A. Chenevas-Paule, P. Duvaut, L. Grenouillet, P. Hollinger, A. Million, G. Rolland, and C. Vannuffel, *Phys. Status Solidi A* **176**, 279 (1999).
- <sup>12</sup>H. P. Xin, C. W. Tu, and M. Geva, *Appl. Phys. Lett.* **74**, 2337 (1999).
- <sup>13</sup>T. Kageyama, T. Miyamoto, S. Makino, F. Koyama, and K. Iga, *Jpn. J. Appl. Phys., Part 2* **38**, L298 (1999).
- <sup>14</sup>P. J. Klar, H. Grüning, J. Koch, S. Schäfer, K. Volz, W. Stolz, W. Heimbrodt, A. M. Kamal Saadi, A. Lindsay, and E. P. O'Reilly, *Phys. Rev. B* **64**, 121203(R) (2001).
- <sup>15</sup>M. Albrecht, V. Grillo, T. Remmele, H. P. Strunk, A. Yu Egorov, Gh. Dumitras, H. Riechert, A. Kaschner, R. Heitz, and A. Hoffmann, *Appl. Phys. Lett.* **81**, 2719 (2002).
- <sup>16</sup>J. Wagner, T. Geppert, K. Köhler, P. Ganser, and M. Maier, *Solid-State Electron.* **47**, 461 (2003).
- <sup>17</sup>E. M. Pavelescu, T. Jouhti, M. Dumitrescu, P. J. Klar, S. Karirinne, Y. Fedorenko, and M. Pessa, *Appl. Phys. Lett.* **83**, 1497 (2003).
- <sup>18</sup>E. Tournie, M. A. Pinault, M. Laugt, J. M. Chaveau, A. Trampert, and K. H. Ploog, *Appl. Phys. Lett.* **82**, 1845 (2003).
- <sup>19</sup>W. Ha, V. Gambin, S. Bank, M. Wistey, H. Yuen, S. Kim, and J. S. Harris, *IEEE J. Quantum Electron.* **38**, 1260 (2002).
- <sup>20</sup>R. Kudrawiec, G. Sek, J. Misiewicz, D. Gollub, and A. Forchel, *Appl. Phys. Lett.* **83**, 2772 (2003).
- <sup>21</sup>H. D. Sun, R. Macaluso, M. D. Dawson, F. Robert, A. C. Bryce, J. H. Marsh, and H. Riechert, *J. Appl. Phys.* **94**, 1550 (2003).
- <sup>22</sup>X. Yang, J. B. Heroux, M. J. Jurkovic, and W. I. Wang, *J. Vac. Sci. Technol. B* **17** (1999).
- <sup>23</sup>S. G. Spruytte, M. C. Larson, W. Wampler, C. W. Coldren, H. E. Petersen, and J. S. Harris, *J. Cryst. Growth* **227–228**, 506 (2001).
- <sup>24</sup>S. Kurtz, J. Webb, L. Gedvilas, D. Friedman, J. F. Geisz, J. M. Olson, R. King, D. Joslin, and N. Karam, *Appl. Phys. Lett.* **78**, 748 (2001).
- <sup>25</sup>J. Wagner, T. Geppert, K. Köhler, P. Ganser, and N. Herres, *J. Appl. Phys.* **90**, 5027 (2001).
- <sup>26</sup>T. Kitatani, M. Kondow, and M. Kudo, *Jpn. J. Appl. Phys., Part 2* **40**, L750 (2001).
- <sup>27</sup>V. Lordi, V. Gambin, S. Friedrich, T. Funk, T. Takizawa, K. Uno, and J. S. Harris, *Phys. Rev. Lett.* **90**, 145505 (2003).
- <sup>28</sup>V. Gambin, V. Lordi, S. Friedrich, T. Funk, T. Takizawa, K. Uno, and J. S. Harris, *J. Cryst. Growth* **251**, 408 (2003).
- <sup>29</sup>G. Ciatto, F. D'Acapito, L. Grenouillet, H. Mariette, D. De Salvador, G. Bisognin, R. Carboni, L. Floreano, R. Gotter, S. Mobilio, and F. Boscherini, *Phys. Rev. B* **68**, 161201 (2003).
- <sup>30</sup>K. Kim and A. Zunger, *Phys. Rev. Lett.* **86**, 2609 (2001).
- <sup>31</sup>H. Ch. Alt, A. Yu Egorov, H. Riechert, B. Wiedemann, J. D. Meyer, R. W. Michelmann, and K. Bethge, *Physica B (Amsterdam)* **302**, 282 (2001).
- <sup>32</sup>K. Leifer, P. A. Buffat, J. Cagnon, E. Kapon, A. Rudra, and P. A. Stadelmann, *J. Cryst. Growth* **237–239**, 1471 (2002).
- <sup>33</sup>K. Volz, O. Rubel, T. Torunski, S. D. Baranovskii, and W. Stolz, *Appl. Phys. Lett.* **88**, 081910 (2006).
- <sup>34</sup>P. A. Doyle and P. S. Turner, *Acta Crystallogr., Sect. A: Cryst. Phys., Diffraction, Theor. Gen. Crystallogr.* **24**, 390 (1968).
- <sup>35</sup>F. Glas, *Philos. Mag.* **84**, 2055 (2004).
- <sup>36</sup>P. N. Keating, *Phys. Rev.* **145**, 637 (1966).
- <sup>37</sup>O. Rubel, K. Volz, T. Torunski, S. D. Baranovskii, F. Grosse, and W. Stolz, *Appl. Phys. Lett.* **85**, 5908 (2004).